AFRL-RZ-WP-TP-2010-2052

MEASUREMENTS OF COMBUSTION PROPERTIES IN A MICROWAVE ENHANCED FLAME (POSTPRINT)

Campbell D. Carter

Propulsion Sciences Branch
Aerospace Propulsion Division

Emanuel S. Stockman, Sohail H. Zaidi, and Richard B. Miles

Princeton University

Michael D. Ryan

Universal Technology Corporation

FEBRUARY 2010

AIR FORCE RESEARCH LABORATORY
PROPULSION DIRECTORATE
WRIGHT-PATTERSON AIR FORCE BASE, OH 45433-7251
AIR FORCE MATERIEL COMMAND
UNITED STATES AIR FORCE

REPORT DOCUMENTATION PAGE

Form Approved
OMB No. 0704-0188

1. REPORT DATE *(DD-MM-YY)*	2. REPORT TYPE	3. DATES COVERED *(From - To)*
February 2010	Journal Article Postprint	01 December 2007 – 01 December 2008

4. TITLE AND SUBTITLE
MEASUREMENTS OF COMBUSTION PROPERTIES IN A MICROWAVE ENHANCED FLAME (POSTPRINT)

5a. CONTRACT NUMBER
In-house

5b. GRANT NUMBER

5c. PROGRAM ELEMENT NUMBER
61102F

6. AUTHOR(S)
Campbell D. Carter (AFRL/RZAS)
Emanuel S. Stockman, Sohail H. Zaidi, and Richard B. Miles (Princeton University)
Michael D. Ryan (Universal Technology Corporation)

5d. PROJECT NUMBER
2308

5e. TASK NUMBER
AI

5f. WORK UNIT NUMBER
2308AI00

7. PERFORMING ORGANIZATION NAME(S) AND ADDRESS(ES)
Propulsion Sciences Branch (AFRL/RZAS)
Aerospace Propulsion Division
Air Force Research Laboratory, Propulsion Directorate
Wright-Patterson Air Force Base, OH 45433-7251
Air Force Materiel Command, United States Air Force

Princeton University
Olden Street
Princeton, NJ 08544

Universal Technology Corporation
Dayton, OH 45332

8. PERFORMING ORGANIZATION REPORT NUMBER
AFRL-RZ-WP-TP-2010-2052

9. SPONSORING/MONITORING AGENCY NAME(S) AND ADDRESS(ES)
Air Force Research Laboratory
Propulsion Directorate
Wright-Patterson Air Force Base, OH 45433-7251
Air Force Materiel Command
United States Air Force

10. SPONSORING/MONITORING AGENCY ACRONYM(S)
AFRL/RZAS

11. SPONSORING/MONITORING AGENCY REPORT NUMBER(S)
AFRL-RZ-WP-TP-2010-2052

12. DISTRIBUTION/AVAILABILITY STATEMENT
Approved for public release; distribution unlimited.

13. SUPPLEMENTARY NOTES
Journal article published in *Combustion and Flame*, Vol. 156 (2009). PA Case Number: 88ABW-2008-0457; Clearance Date: 06 Oct 2008. Paper contains color. © 2009 The Combustion Institute. The U.S. Government is joint author of this work and has the right to use, modify, reproduce, release, perform, display, or disclose the work.

14. ABSTRACT
Microwave induced flame speed enhancement is quantified in a laminar, premixed CH4/air wall stagnation flat flame. Experiments were performed in a high Q microwave cavity with the cavity tuned so that the maximum microwave field is located in the vicinity of a flat flame front. Equivalence ratios were varied between 0.6 and 0.8. When the flame is radiated by a continuous wave microwave field of approximately 5 kV/cm, the flame front is observed to move towards the burner exit and stabilize at a standoff distance corresponding to a flame speed increase of up to 20%. No microwave discharge is observed, indicating that the enhanced flame speed arises from microwave energy deposited directly into the reaction zone through coupling to the weakly ionized gas in that region. Laser diagnostics were performed to quantify temperature increase, the laminar flame speed enhancement, and changes in the OH radical concentration through filtered Rayleigh scattering, particle image velocimetry, and planar laser induced fluorescence, respectively.

15. SUBJECT TERMS
Hydrocarbon combustion, Microwave, Electric field, PIV flame speed, Rayleigh temperature, OH–PLIF, Plasma assisted combustion

16. SECURITY CLASSIFICATION OF:			17. LIMITATION OF ABSTRACT:	18. NUMBER OF PAGES	19a. NAME OF RESPONSIBLE PERSON (Monitor)
a. REPORT	b. ABSTRACT	c. THIS PAGE			Campbell D. Carter
Unclassified	Unclassified	Unclassified	SAR	16	19b. TELEPHONE NUMBER *(Include Area Code)* N/A

Standard Form 298 (Rev. 8-98)
Prescribed by ANSI Std. Z39-18

Combustion and Flame 156 (2009) 1453–1461

Contents lists available at ScienceDirect

Combustion and Flame

journal homepage: www.elsevier.com/locate/combustflame

Measurements of combustion properties in a microwave enhanced flame

Emanuel S. Stockman [a,*], Sohail H. Zaidi [a], Richard B. Miles [a], Campbell D. Carter [b], Michael D. Ryan [c]

[a] Engineering Quadrangle – Mechanical and Aerospace Engineering, Olden Street, Princeton University, Princeton, NJ 08544, USA
[b] U.S. Air Force Research Laboratory, Wright-Patterson Air Force Base, Dayton, OH 45433, USA
[c] Universal Technology Corporation, Dayton, OH 45332, USA

ARTICLE INFO

Article history:
Received 7 October 2008
Received in revised form 27 January 2009
Accepted 20 February 2009
Available online 13 May 2009

Keywords:
Hydrocarbon combustion
Microwave
Electric field
PIV flame speed
Rayleigh temperature
OH–PLIF
Plasma assisted combustion

ABSTRACT

Microwave induced flame speed enhancement is quantified in a laminar, premixed CH_4/air wall stagnation flat flame. Experiments were performed in a high Q microwave cavity with the cavity tuned so that the maximum microwave field is located in the vicinity of a flat flame front. Equivalence ratios were varied between 0.6 and 0.8. When the flame is radiated by a continuous wave microwave field of approximately 5 kV/cm, the flame front is observed to move towards the burner exit and stabilize at a standoff distance corresponding to a flame speed increase of up to 20%. No microwave discharge is observed, indicating that the enhanced flame speed arises from microwave energy deposited directly into the reaction zone through coupling to the weakly ionized gas in that region. Laser diagnostics were performed to quantify temperature increase, the laminar flame speed enhancement, and changes in the OH radical concentration through filtered Rayleigh scattering, particle image velocimetry, and planar laser induced fluorescence, respectively. These measurements indicate that microwave radiation may prove to be an effective means to non-invasively control and enhance flame stability in combustors.

1. Introduction

Over the past few decades, several research groups have investigated the potential for a system in which microwave energy couples into and positively affects a combusting flame front. The field of microwave enhanced combustion can be classified under the larger subject area of plasma assisted combustion. Within this area, the research topics range from studying how plasmas in the reactant flow may provide reduced ignition delay times to how electric fields themselves may couple into the low density plasma within the thin reacting flame front. The research presented here falls into the latter category, as microwaves have limited ability to interact with uncharged reactant species. Many articles have been published over the years debating the potential for both electric-field and microwave enhanced flames [1–7]. Studying this literature, one can see that for each published experimental result that demonstrated improved flame performance and stability, there appears to be another that claimed failure at reproducing the reported effect. A review of the field of electrically enhanced flames shed light on some of the challenges associated with this research area and provided guidance in the design of a reliable microwave enhanced laminar flame testbed.

Seminal work performed in the early 1950s by Calcote [8] demonstrated that sub-breakdown electric fields were able to interact with the propagation of a laminar tube flame and significantly improve flame blowoff stability. Fowler later reported a 50% increase in the propagation velocity of a natural gas/air flame, as measured by a time of flight diagnostic [9]. Similar work with electrode generated fields was undertaken by Jaggers [1] and Bowser [2]. Their research reported that direct current (DC) fields produced no discernable increase in burning velocity in tubular and stationary flames. Jaggers recognized that DC operation was inherently complicated in that it would be difficult to separate a kinetic flame speed enhancement from a simple ion wind forcing of the flame. As an alternative, he proposed and investigated the effect of 50 MHz high-frequency radiation on flame propagation, and he successfully measured a 20% increase in flame speed in CH_4/air flames. Ward and Wu followed with a theoretical paper that stated that a move towards even higher frequency radiation would enable the use of resonant microwave cavities to generate stronger electromagnetic fields [3].

Circular and rectangular cylinder geometries are typically used in resonant microwave cavities, and configurations with combustion systems are possible because characteristic lengths of many laminar burner devices are on the order of microwave wavelengths. Operating the microwave cavity on resonance can, if desired, generate electric fields above the breakdown threshold of air without the use of invasive electrodes. However, the main drive of the research presented here is to examine the coupling of the microwave energy with the flame zone itself at field strengths below this threshold. After the publication of Ward's

* Corresponding author.
E-mail address: estockma@princeton.edu (E.S. Stockman).

0010-2180/$ - see front matter © 2009 The Combustion Institute. Published by Elsevier Inc. All rights reserved.
doi:10.1016/j.combustflame.2009.02.006

hypothesis, several research groups designed experiments to examine the effects of microwave radiation on flames. Early work by Clements in a high quality-factor (Q-factor) cavity claimed 20% enhancement in flame speed with fields near 2000 V/cm [10]. Additional research published 1 year later by MacLatchy and Clements [4] was unable to reproduce the result and conceded the difficulty in making a definite conclusion of a positive interaction. The inherent difficulty in designing a testbed that permitted both microwave stability and accurate combustion diagnostics prevented any conclusive statement from being formulated. Even more recent research from Groff and Krage [5] and Ogawa et al. [11] failed to clarify the issue. Groff designed an excellent microwave cavity based on his extensive knowledge of the field but appeared to have difficulty with the diagnostics and with the design of a burner that could generate a stable flat flame for accurate characterizations. The experiments by Ogawa et al. seemed to have the most thorough setup to date. They measured a 180% increase in the electron temperature of the flame front but did not attempt to take measurements of flame speed. Thus, it is our belief that there is a need for further study of microwave enhanced combustion and that success will depend upon a careful integration of combustion, electromagnetics, and diagnostics.

Employing a microwave waveguide-generated electric field mitigates the ionic wind issues that have added much confusion in the interpretation of DC electrode enhanced flame experiments. Whereas Starikovskii [12] attributes almost all effects seen in these DC systems to the mechanical body force of the electric field on positive ions, Marcum and Ganguly [13] counters such an explanation and suggests an 'electric pressure' modification of ion Lewis number. Fortunately, neither of these theories is applicable to a microwave enhanced flame. Since the standing wave electric field oscillates in polarity at the microwave frequency, which for our experiments is 2.45 GHz, none of the effects that are observed can be attributed to the ionic wind. Eliminating the ionic wind body force as a potential mechanism for the observed movement in microwave enhanced flames does not significantly reduce the complexity of the interaction. With strong electric fields, the processes of gas excitation, ionization, and chemiionization all become relevant. As discussed by Pedersen and Brown [6] and Ju et al. [14], free electrons in a CH_4/air flame are primarily created by the chemiionization reaction,

$$CH + O \rightarrow HCO^+ + e^-,$$

and are confined to the narrow, fast reacting flame front. The microwave generated electric field is therefore expected to deposit most of its energy in this region since it can only couple to charged particles. If the electron temperature is significantly increased by the deposited microwave energy, then the electron–molecule collisions will proceed to increase the gas temperature. It is at this level of understanding where the plasma combustion community has had difficulty explaining the flame interaction that follows this coupling. The observation of a flame speed increase in the microwave enhanced combustion system can be explained in one, or some combination, of the following three ways: (1) the transfer of energy from the electrons to the flame species through collisions acts as a method of localized gas heating and enthalpy addition, (2) the microwave driven electrons couple directly to the vibrational modes of molecules such as oxygen and provide enhanced reactivity, and/or (3) the microwave field directly affects chemical reactions by activating certain species that become important in complete plasma combustion mechanisms. All three of these scenarios offer the ability to couple energy directly into a flame front, although the first may be more efficiently achieved by preheating the reactants. This paper does not undertake to establish a theory but demonstrates that microwave enhanced flame effects are present and seeks to present an accurate and thorough set of laser diagnostic measurements of these effects.

Results on this testbed were first reported by Zaidi et al. [15], who used a microwave cavity configuration that is similar to the one used in our experiments. Their first observation of the enhanced flame estimated increases in flame speed of over 30% for a CH_4/air flame, and the work herein continues this past research to accurately quantify the system. Experimental results from a series of laser diagnostics performed on the microwave enhanced combustion testbed show a significant increase of the laminar flame speed of a premixed CH_4/air flat flame generated by a burner with exit diameter, D_e, and stagnation plane standoff distance, L_e. The continuous wave (CW) microwave radiation generates 5 kV/cm electric field strengths, and coupling between the resonant microwave energy and the flame is observed to reposition the flat flame almost one L_e/D_e units closer to the burner exit with only a few watts of absorbed power. Particle image velocimetry (PIV) measurements of the enhanced, reacting flow field provide quantitative two-dimensional velocity measurements of the flame speed enhancement. The PIV work is complemented by measurements of axial gas temperature using filtered Rayleigh scattering (FRS). The temperature increase downstream of the flame provides a measure of the total power added in the flame zone by microwaves. In addition, OH concentration is measured using planar laser induced fluorescence (PLIF).

The complex nature of electric field interactions does not easily lend itself to standard methods of flame diagnostics. For example, intrusive probes such as thermocouples and Langmuir probes cannot be used since they interact with the microwave field. Each diagnostic of the experiment was chosen for its non-invasive characteristic and for the important combustion or flow property it would interrogate. The quantification of the observed flame speed increase by PIV is the key parameter of these experiments as it provides definitive evidence of the extent of the flame speed enhancement. Combined with the other diagnostics, axially resolved data provide valuable insight on whether the enhancement mechanism occurs due to an interaction within the flame front or one that is being propagated from the downstream gases. Additionally, the flame speed data may serve to validate future models of the interaction. The FRS temperature diagnostic along the flame axis is used to identify the location of the energy addition and to quantify any spatial changes in the post-flame gas temperature that may suggest the possibility of either a change in flame chemistry or a bulk heating of the post-flame zone hot gases. PLIF provides a full two-dimensional profile of OH-number density for insight regarding the location and mechanism for the microwave enhanced flame interaction. Flame speed enhancement through thermal, vibrational, or chemical processes associated with microwave energy deposition all originate with microwave coupling to the low density plasma and charged flame species, albeit through different mechanisms. The ability to discern the relative dominance of each mechanism will require the measurement of major combustion species, intermediate species and energy level populations, which have not been undertaken in this study. The results of the combined diagnostic suite presented here are intended to provide plasma assisted combustion modeling efforts with three validation parameters to incorporate into their research towards establishing the various mechanisms of microwave and electrically enhanced flames.

2. Experimental setup

The key developments of the experiment came in the design of a testbed that would not sacrifice the precision of combustion laser diagnostics to the need for stable, high Q-factor, single-mode

microwave operation. The burner is a single jet stagnation system similar to that used by Egolfopoulos et al., and has been shown to be an excellent testbed for analyzing combustion performance [16]. Holes for optical access create discontinuities on the waveguide surface that become potential sources for propagation of non-TE_{10} modes. Therefore, every machined hole in the microwave cavity is no larger than 3 cm to prevent leakage of the 2.45 GHz radiation. The configuration in Fig. 1 depicts the experimental layout and shows optical access for both planar and burner-axial laser diagnostics. The three laser diagnostics were not performed simultaneously due to minimal optical access in the cavity. All experiments were conducted at atmospheric pressure.

2.1. Burner operation

The stagnation flame system produces one planar, steady laminar flame that can be used to study flame speed and flame standoff positions. The burner used in the experiments has a contoured central nozzle (D_e = 15 mm) with a concentric coflow of nitrogen to prevent air entrainment and improve stability. A volume of glass beads at the base of the center nozzle sufficiently laminarizes the gas to provide nearly uniform flow out of the exit. The 25 mm thick, water-cooled, aluminum ceiling of the microwave cavity test section is used as the flame stagnation surface at a distance, L_e, of 5.46 cm from the burner exit. At low strain rates and large flame standoff distances, these types of flames are not significantly affected by heat conduction to the stagnation surface [16]. The flame is stabilized in the strained flow field by the aerodynamic strain rate and the large L_e/D_e ratio of the burner system limits the range of attainable CH_4/air flames to equivalence ratios between 0.60 and 0.85. Total volumetric flow rates were between 3 and 10 slpm (273.15 K reference temperature). A set of sonic nozzles controlled the flow of each gas and were calibrated with a DryCal piston-type flow meter to 1% accuracy.

2.2. Microwave system

The rectangular cross-section waveguide contains and propagates radiation from the Panasonic 1.3 kW, 2.45 GHz, CW magnetron (Model 2M261-M32) to generate a stable TE_{10} mode structure in the WR430 (10.92 cm × 5.46 cm) test section. The standing mode of the TE_{10} electric field is linearly polarized along the flame axis (y-axis) and its amplitude undergoes a sinusoidal oscillation along the z-axis with a guide wavelength of λ_g = 14.8 cm. The sliding short was adjusted to position a local maximum of the electric field along the flame axis as in Fig. 1. The 3-stub tuner was then used to tune to resonance Q-factors up to 200. Measuring the electric field strength at the location of the flame is difficult as any invasive probe technique would spoil the Q-factor. Instead, an approximation can be made from the TE_{10} mode structure using the following equations

$$P_{MW} = \frac{1}{\eta_{TE}} |E_o|^2 ab \sqrt{1 - \left(\frac{v_c}{v_o}\right)^2}, \tag{1}$$

$$|E_o|^2 \approx Q P_{MW} \eta_{TE} \left[ab \sqrt{1 - \left(\frac{v_c}{v_o}\right)^2} \right]^{-1}, \tag{2}$$

where P_{MW} is the continuous microwave power, η_{TE} is the transverse mode impedance, E_0 is the maximum single-pass electric field strength, and v_c and v_o are the cutoff and radiation frequencies of the system, respectively [17]. The Q-factor for the unloaded microwave waveguide was measured on a Hewlett Packard 8720C network analyzer to be between 100 and 200. With the 1.3 kW source and at high Q-factor, breakdown is easily generated in the burnt gas region of the flame. To avoid breakdown, the cavity Q-factor is reduced by detuning from the highly resonant condition with the 3-stub impedance matching waveguide device. The actual operation point of the microwave enhanced combustion experiment is between 10 and 50. Using Eq. (2), the electric field under these conditions is approximately 5 kV/cm and is polarized in the y-direction of Fig. 1. This electric field orientation is perpendicular to the flat flame front and oscillates in direction at 2.45 GHz. The rapidly changing polarity of the electric field at the flame removes concern over ion wind forcing effects that can confuse experiments using DC electrode generated electric fields [4,13,18]. Additional details regarding microwave propagation and waveguide mode structures can be found in Gandhi [17].

2.3. Laser diagnostics

Optical access and low signal levels prevent simultaneous PIV, FRS, and PLIF measurements. Instead, the diagnostics were performed in separate experiments, with microwave and flame operating conditions replicated as best as possible. In each case the Bios DryCal was used to ensure repeatability of flow conditions. In the PIV and PLIF experiments, laser access was achieved through the vertical slits (Fig. 1i) for planar interrogation while FRS utilized the hole in ceiling of the cavity (Fig. 1k) for beam measurements. Scattering and fluorescence were collected through a 5 cm × 2 cm window in the microwave cavity that is covered with a metallic mesh to prevent microwave leakage. The effect of imaging through a meshed window is taken into account by flat-field normalization in both FRS and PLIF.

2.3.1. PIV diagnostics

Recent publications have demonstrated the benefit of PIV for instantaneous flame speed and velocity gradient diagnostics specifically on stagnation flame systems [19,20]. More detailed descriptions of PIV procedures and theory can be found in Raffel et al. [21]. The PIV experiments performed on the microwave enhanced flame use a TSI configured system and Buehler 0.5 μm

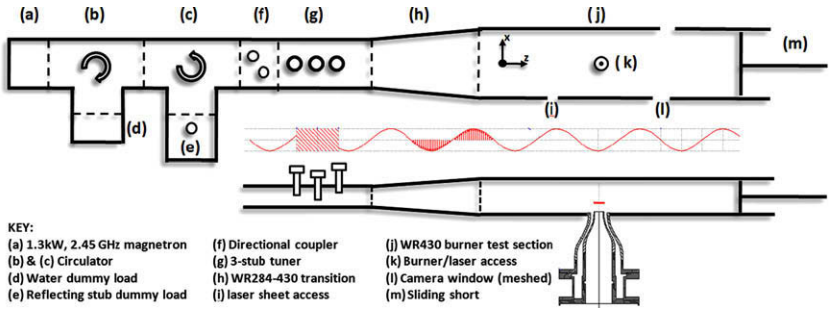

Fig. 1. Schematics of cavity resonator for the microwave enhanced combustion experiments. The superimposed plot of the tuned TE_{10} mode shows a maximum electric field at the flame front.

diameter alumina particles for flow seeding. The TSI PowerView Plus camera images a 33 mm × 33 mm cross-section of the flow field onto the 2048 pixel × 2048 pixel CCD for a resolution of 16.28 μm/pixel. The camera is equipped with a Nikon 105 mm lens with its *f*-stop set to *f*/5.6. A 532 nm narrow bandpass filter is used to block flame luminosity. The seed particles are illuminated by a New Wave Solo Nd:YAG PIV laser that is capable of generating two 30 mJ laser pulses (wavelength = 532 nm) at a repetition rate of 7.5 Hz. The two laser pulses, typically separated by 500 μs, are directed through a Keplerian-type beam expander (6×) and laser sheet forming optics before passing through the narrow laser slits of the waveguide test section. The 500 μm thick laser sheets intersect the reacting flow field so that the flow axis is wholly contained in the cross-section and both axial and radial velocity vectors could be calculated. Image pairs are processed using the cross-correlation technique of the Insight 3G software package. The correlation uses a 1.05 mm × 1.05 mm interrogation box with a maximum 50% overlay factor to resolve the planar velocity field. The output of this software provides axial velocity information from the exit of the burner up until the flame zone; the particle density is not large enough to resolve post-flame velocities. Furthermore, as the flame front is approached, thermophoretic effects act to bias the derived velocities [22] and are considered within the experimental error of this experiment. The reference flame speed is derived as per the method detailed by Law et al. [20] as the minimum point in the axial velocity profile.

2.3.2. FRS diagnostics

As initially demonstrated by Miles et al. [23], the application of FRS is especially suitable to environments where laser scattering from surfaces and dust particles significantly interfere with the Rayleigh signal. When illuminated by a narrow linewidth laser, molecular gases elastically scatter an acoustically and thermally broadened Rayleigh–Brillouin signal. If imaged through the appropriate molecular filter with the laser tuned to the center of the filter absorption line, much of this thermally broadened Rayleigh–Brillouin signal is still transmitted while background scattering at the laser wavelength is strongly attenuated. In a constant pressure environment like the microwave enhanced combustion testbed, the laser can be tuned to an optimal frequency so that the collected FRS signal has a monotonic dependence on temperature. The diagnostic was successfully applied to a premixed CH_4/air flame by Elliott et al. [24] and shown to measure flame temperatures to within 5% accuracy.

In the microwave enhanced combustion experiment, optical access for FRS laser diagnostics is achieved through a 3 mm diameter hole in the stagnation ceiling. The laser is directed along the flame axis into the burner itself, which serves as the beam dump. Although the surface reflections from the burner generate an undesirable level of background scattering, the FRS method provides ample attenuation of the narrow linewidth background scattering. The laser employed in the FRS temperature diagnostic is a frequency doubled, Nd:YAG Spectra Physics GCR-170 that generates 300 mJ/pulse at 10 Hz. The laser is equipped with an injection seeder unit to provide narrow linewidth (100 MHz) and tunability across a range of I_2 transitions. To achieve the necessary suppression of the background wall scattering in the microwave cavity, the laser is centered on an optically thick I_2 absorption line at 18787.8 cm^{-1}. An I_2 vapor cell with length 16.5 cm is run with a cold tip temperature of 317.5 K and positioned in front of a Princeton Instruments PI-MAX HQf GEN III ICCD camera that images the Rayleigh scattering from the flame region. Images are collected on the 512 pixel × 512 pixel PI-MAX with a 300 ns time gate to mitigate interference from flame luminosity. To reduce noise and improve signal levels, the CCD images are binned 2 × 2 before readout. The final resolution of 120 μm/pixel is sufficient to resolve flame front temperatures and relevant dimensional scales in the reaction zone.

The 16-bit raw image pixel intensities can be related to temperature measurements by simulating the filtered Rayleigh–Brillouin scattering signal from the gases in the interrogated region [25]. The total Rayleigh–Brillouin scattering intensity from a mixture of L combustion species is given by

$$R_{\mathrm{tot}}(\bar{\nu}, T_{\mathrm{g}}) = C I_0 N \sum_{i=1}^{L} \chi_i \sigma_i r_i(\bar{\nu}, P, T_{\mathrm{g}}, M_i), \tag{3}$$

where C is a function of the optical setup, I_0 is the laser intensity, N is the total gas number density, and T_g is the interrogated gas temperature. The species specific mole fraction, scattering cross-section, and Rayleigh–Brillouin scattering profile are given by the parameters, χ_i, σ_i, and $r_i(\bar{\nu},\ P,\ T_{\mathrm{g}},\ M_i)$. A common practice with FRS on premixed flames is to ignore the unknown gas composition and assume a single component mixture of nitrogen. This approximation led to about a 5% error in the study of Elliott et al. [24]. Relative temperature changes can be measured at much better accuracy, and because the purpose of the FRS diagnostic in the microwave combustion experiment is to quantify changes in gas temperature of the enhanced flame, this approximation was used. As demonstrated in Fig. 2, the total signal detected by the camera is modeled as the integration of the Rayleigh–Brillouin scattering that is transmitted through the I_2 absorption cell,

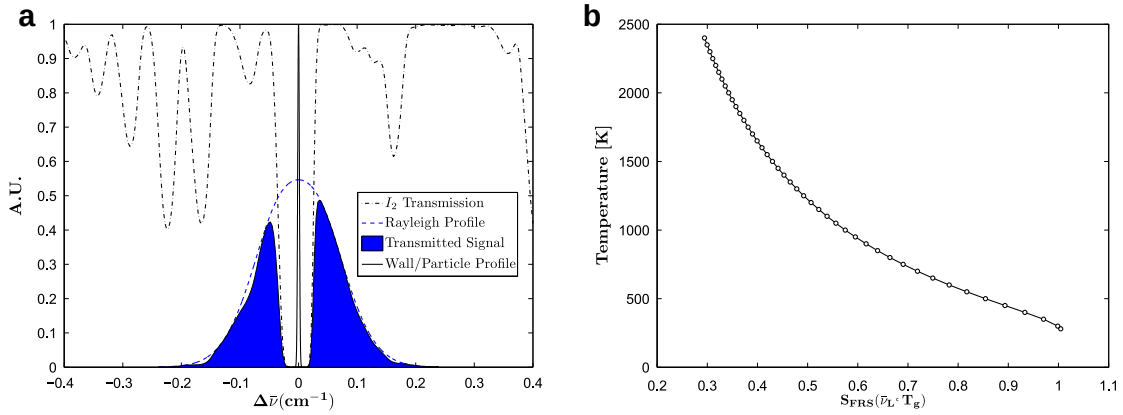

Fig. 2. (a) Simulated filtered Rayleigh–Brillouin scattering profile of N_2 gas at 1800 K overlaid with the I_2 gas cell transmission profile at 318.5 K. (b) This integrated signal, when normalized by a cold gas signal provides a monotonic relationship to gas temperature.

$$S(\bar{\nu}_L, T_g) = \int_{-\infty}^{\infty} R_{N_2}(\bar{\nu}, T_g)\tau(\bar{\nu}_L - \bar{\nu})d\bar{\nu}$$
$$= CI_0 N\sigma_{N_2} \int_{-\infty}^{\infty} r_{N_2}(\bar{\nu}, P, T_g, M_{N_2})\tau(\bar{\nu}_L - \bar{\nu}), \quad (4)$$

where $\tau(\bar{\nu})$ is the I_2 transmission profile, $\bar{\nu}_L$ is the wavenumber of the interrogation laser, and $R_{N_2}(\bar{\nu}, T_g)$ is the Rayleigh–Brillouin scattering profile of nitrogen gas given in Eq. (3). By normalizing the simulated FRS signals to that from room temperature air, the optical constant, C, and laser intensity, I_0, are removed from the calculation. A model was developed for the ratio,

$$S_{\mathrm{FRS}}(T_g) = \frac{S(\bar{\nu}_L, T_g)}{S_{\mathrm{air}}(\bar{\nu}_L, T_{\mathrm{amb}})\frac{\sigma N_2}{\sigma_{\mathrm{air}}}}, \quad (5)$$

that can be used to a quantify measurements taken in the laboratory. The FRS temperature model used in this experiment, for illumination at 18787.8 cm^{-1}, is shown in Fig. 2.

2.3.3. OH–PLIF diagnostics

Given that the temperature range of the experimental burner is between 1700 and 2100 K, the OH $Q_1(8)$ $A^2\Sigma^+$–$X^2\Pi$ (1,0) transition was selected for interrogation because of the insensitivity of its ground state Boltzmann population fraction over the expected temperatures. The PLIF facility uses a frequency doubled, Spectra Physics GCR-170 Nd:YAG laser to drive a Lumonics HD-300 dye laser system at 10 Hz. The laser, operating with Rhodamine 590, produces a 70 mJ laser beam at 567.106 nm before entering an Inrad Autotracker III for second harmonic generation. The frequency doubled laser radiation at 283.55 nm for $Q_1(8)$ excitation is separated from its fundamental with an Inrad Harmonic Separator. The final beam energy of 14 mJ/pulse is split into two paths. A portion of the beam (~4%) is directed to a reference flame to track and maintain $Q_1(8)$ tuning and then to a photodiode (to track beam energy). The remainder of the beam is propagated through laser sheet forming optics before entering the optical access slits in the microwave cavity. The combination of a −100 mm plano-concave cylindrical lens and 600 mm spherical lens, in a telescope arrangement, generate a 300 μm thick laser sheet at the center of the axisymmetric flame. The fluorescence from the flame is collected on a PI-MAX Superblue ICCD camera. The camera is equipped with a Cerco 45 mm UV lens at f/1.8 and the resulting images have a resolution of 150 μm/pixel after binning pixels 2 × 2. Schott WG305 and UG5 glass filters are used to transmit the fluorescence from the A–X (1,1) and A–X (0,0) bands above 310 nm and also fully attenuate the A–X (1,0) fluorescence and background scattering around 283 nm.

In the PLIF regime of this experiment, the number density of OH radicals is proportional to the collected PLIF and can be quantified by referencing a nearly adiabatic burner operating at similar conditions. Calibration for the OH–PLIF diagnostic is performed with a Hencken burner (Technologies for Research Model RT1x1) in a premixed mode with a $\phi = 0.95$ CH_4/air mixture. The Hencken burner generates a nearly adiabatic flame and past literature has reported a temperature of 2170 K and a OH-number density of $(0.94 \pm 0.07) \times 10^{16}$ cm^{-3} at a location 25.4 mm above the Hencken burner surface [26]. The Hencken burner temperature and collisional environment are similar to those of the experimental stagnation flame and thus the variation in electronic quenching rates between the two flames is small; furthermore, laser excitation rates are such that some degree of transition saturation is expected. Thus, together with the nominal change in the $Q_1(8)$ Boltzmann fraction at these temperatures, a simplified equation for OH-number density can be used [27],

$$N_{\mathrm{OH}} = N_{\mathrm{OH,\,cal}} \frac{S_f}{S_{f,\,\mathrm{cal}}}, \quad (6)$$

where N_{OH} is the number density of the OH radical, S_f is the signal intensity collected by the camera, and the 'cal' subscript refers to the calibration burner values.

A 300 image average of the PLIF signal from the Hencken flame is used for the calculation of OH-number density of the microwave enhanced flame from Eq. (6). The Hencken burner is aligned with the microwave cavity so that its PLIF signal is captured through the same meshed window as the experimental stagnation flame. By configuring the calibration burner in this way, a near flat-field response of the camera can be generated and used to normalize any optical collection factors. The OH-number density is often taken to be constant in the vertical direction from the Hencken burner surface [26]. However, a change in the target value of

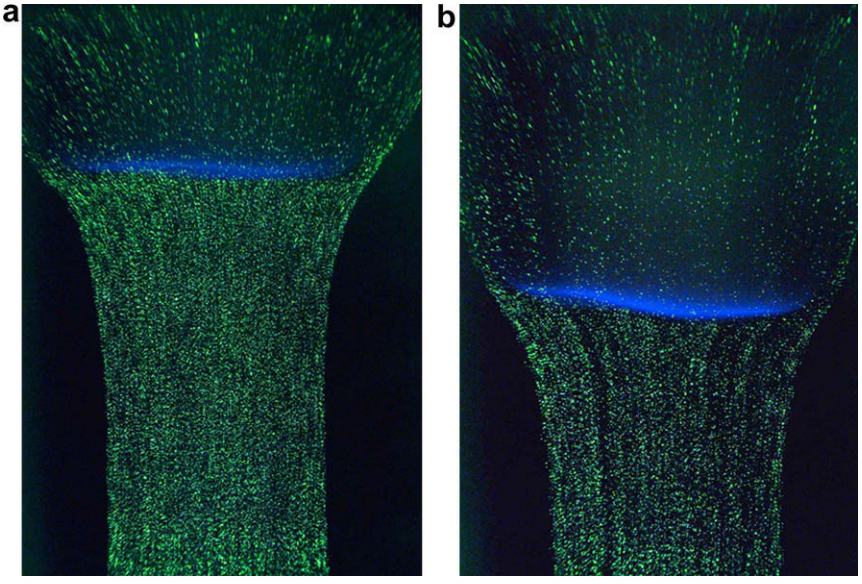

Fig. 3. Two PIV images qualitatively showing the flame speed enhancement. (a) CH_4/air flame, $\phi = 0.78$, (b) the same flame with 1.3 kW of microwave radiation. The flow direction is towards the top of the image with the burner exit at the bottom of the figure and the stagnation plate at the top. Exposure time in these images was purposely lengthened to identify flame front for the figure.

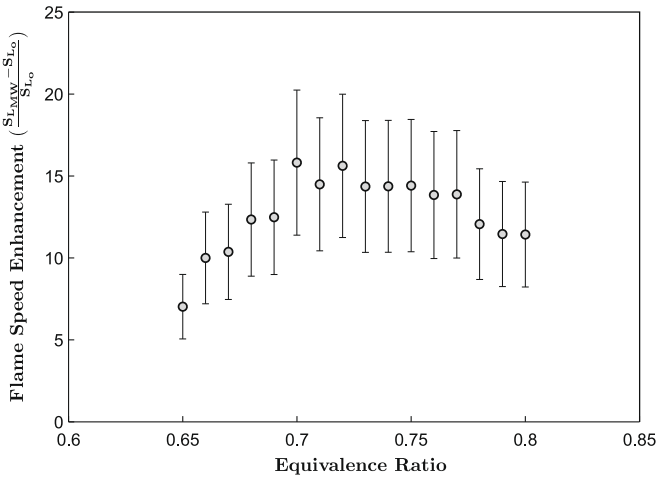

Fig. 4. Variation in flame speed enhancement with equivalence ratio in a premixed CH_4/air flame.

0.94×10^{16} cm^{-3} at 25.4 mm to 0.85×10^{16} cm^{-3} at 40 mm was measured in previous absorption experiments to expected ±10% accuracy. The decay is likely due to radiative effects and this non-uniformity in the Hencken burner OH concentration profile is taken into account in the final calculation of experimental values.

3. Results and discussions

Flame speed enhancements were generated with the careful alignment of the microwave cavity tuning devices. An optimal configuration was set with the sliding short and 3-stub tuning devices by maximizing the power coupled into an antenna at the location of the flame and minimizing the reflected power from the combustion test section. Although the cavity could be easily tuned to induce the breakdown of air, this was avoided. With the 2.45 GHz magnetron generating electric field strengths near 5 kV/cm at the flame, the microwaves are observed to have a pronounced effect on the flame as shown by PIV imaging in Fig. 3. These images show that the microwave enhanced flame of Fig. 3b stabilizes at a location of the flow where the flow velocity is higher, a quantitative sign of an increase in flame speed. The combusting front remained at this location while the microwave power was applied and when the microwave radiation was turned off, the flame immediately returned to its original position with a time response less than 100 ms, but not faster than the characteristic flow time of 25 ms.

The corresponding enhancement in strained flame speed of the flame depicted in Fig. 3 was measured with PIV to be 12.1%. The only mechanism by which the microwave generated electric field can impart such an effect is through a coupling to charged species in the narrow flame front and post-flame gases. The microwave enhanced flame of Fig. 3b appeared slightly distorted from its flat shape, indicating, presumably, a slight non-uniformity of the effect throughout the flame most likely arising from a non-uniformity in the electric field across the volume. As discussed by Ju et al. [14], the electron number density in a lean flame increases significantly with equivalence ratio, and the magnitude of any microwave enhancement in the flame's chemical kinetics should reflect this trend as the electric field can only interact with charged particles. The results of the investigation of microwave flame speed enhancements at several lean equivalence ratios are shown in Fig. 4. Each data point represents the measured increase in strained flame speed when the microwave radiation is activated. A typical dataset at one equivalence ratio was derived from the average flame speed of 20 PIV image pairs of the enhanced flame and another 20 PIV image pairs of the flame as soon as the radiation was terminated. Because the flames stabilize in the same stretched flow field and only relative changes were desired, no extrapolation to a zero strain rate adiabatic flame speed was needed. The precision of these flame speed measurements was better than ±2% as measured by standard deviation of the calculated results. This precision demonstrates both the stability of the flame speed enhancement as well as the capabilities of the PIV system. Each value in Fig. 4 is an average percentage enhancement of at least three datasets. A peak increase in flame speed of 16% occurs at an equivalence ratio of 0.72; although it should be noted that the magnitude of the enhancement was very dependent on the alignment of the resonant microwave cavity. The large error bars represent the range of the average flame speed calculation at a specific equivalence ratio over the three datasets taken on separate days.

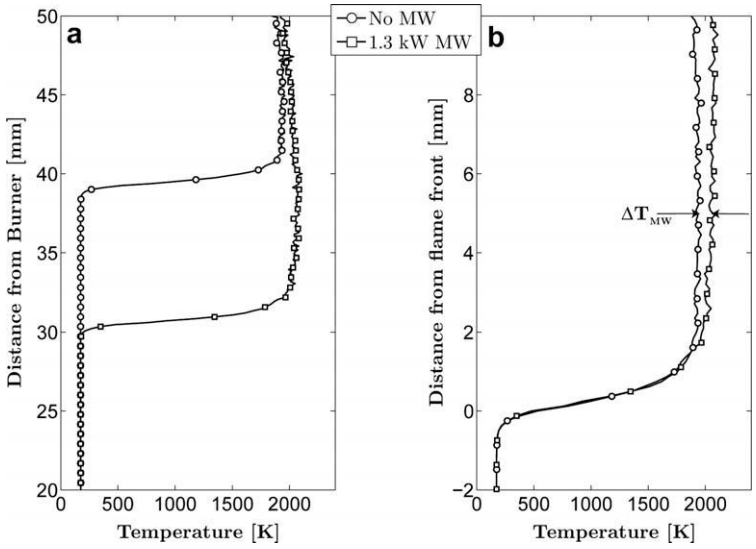

Fig. 5. FRS temperature profiles demonstrating the change in temperature when microwave energy is coupled to enhance the flame speed of a $\phi = 0.75$, CH_4/air flame. (a) Absolute coordinates showing enhanced flame position and equilibration of temperature. (b) Flame shifted coordinate system displaying ~125 K increase in temperature just out of the flame front.

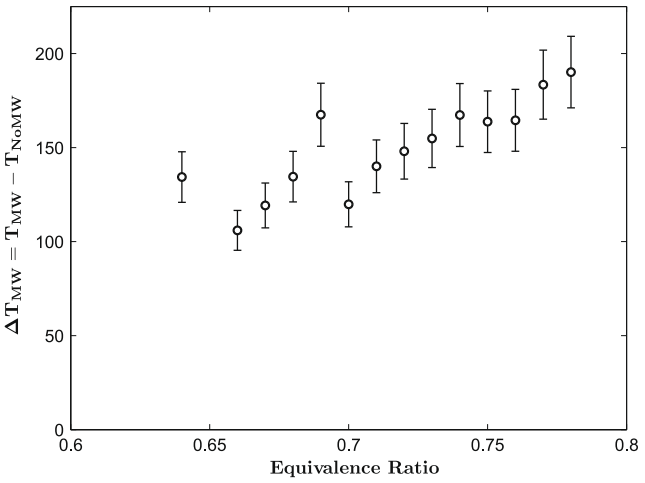

Fig. 6. Measured increase in post-flame gas temperature via microwave enhanced combustion vs. equivalence ratio.

The heating of the cavity by the flame led to a dynamic tuning problem, and flame speed enhancements were measured as low 5% and as high as 21%.

The thermal effects of the microwave interaction with the premixed flame were measured by the FRS diagnostic along the centerline of the flow in the axial direction of the flame. A typical temperature profile of the flame is shown in Fig. 5 where the parameter, ΔT_{MW}, corresponds to the temperature increase associated with the application of the microwaves. Each profile of the ϕ = 0.75, CH_4/air flame in Fig. 5 is the average of 300 instantaneous FRS temperature calculations along the propagation axis of the flame. Several features of the temperature profiles in Fig. 5 are worth noting. First, the FRS temperature of the reactant gases is less than room temperature due to a systematic error in referencing the cold CH_4/air mixture to nitrogen in Eq. (5). Second, there is no increase in the temperature of the cold reactant gases of the microwave flame and therefore the flame speed enhancement is not arising from an increase in initial reactant enthalpy. Lastly, there is a significant increase in temperature throughout the post-flame zone. The temperature of both the non-enhanced and enhanced flames flattened out and equilibrated just after the flame front, not further downstream where the microwave electric field is less likely to deposit its energy, being a region of much lower ion density. This suggests that it is within the flame front, where the electron number density is expected to be at its maximum, that the microwave is coupling and depositing its energy. The equilibration of the temperature enhancement within a few millimeters of the flame front indicates that the microwave enhancement is not volumetrically heating the bulk post-flame gases over the entire length of the 2 cm post-flame region, as hypothesized by Groff anf Krage [5].

The increase in post-flame gas temperature of the microwave enhanced flame, ΔT_{MW}, was averaged over several runs at each equivalence ratio. A *run* is the average of 300 scattering images from the flame with microwave enhancement and immediately after the radiation is turned off. The results of the average increase in temperature at each equivalence ratio are plotted in Fig. 6 with error bars of approximately 15% to exhibit the fluctuations seen in ΔT_{MW} over the course of several runs, not the overall accuracy of the FRS diagnostic. The greatest increase in temperature was seen in a ϕ = 0.78, CH_4/air flame and the measured values of ΔT_{MW} steadily decreased with decreasing equivalence ratio towards the lean limit of the burner. The measured increases in post flame gas temperature of 100–200 K are indicative of the significant flame speed enhancements quantified in Fig. 4. With an estimate of the specific heat and flow rates of the burnt gases, the FRS measured temperature increase can be used to approximate the amount of microwave energy absorbed into the enhanced flame. For a typical flame condition, the increase of 150 K in the post-flame gases corresponds to approximately 20–40 W of absorbed microwave power, approximately 10% of the 300 W combustion power of these flames.

Although the PLIF images are processed into two-dimensional maps of OH-number density as in Fig. 7, the PLIF data are analyzed along the flame centerline in order to compare it to the PIV and FRS datasets. Similar to the data analysis methods of FRS, each OH–PLIF measurement at a specific equivalence ratio and microwave condition consisted of a set of 200 images. The centerline OH profile for each of these 200 instantaneous images was calculated using the Hencken burner for calibration, and then aligned in a flame front coordinate system before being averaged. Even though the variation in flame position was less than 1.5%, the alignment of the OH profiles before averaging proved to be important for resolving the superequilibrium concentration of OH within the flame front. The uncertainty in the OH-number densities is estimated to be ±20%, however, the precision over 200 images of the measurements was typically better than ±5%, even in the flame front. The ability to consistently resolve the peak concentrations of OH enabled the comparison of the slight increases in the parameter for microwave enhanced flames.

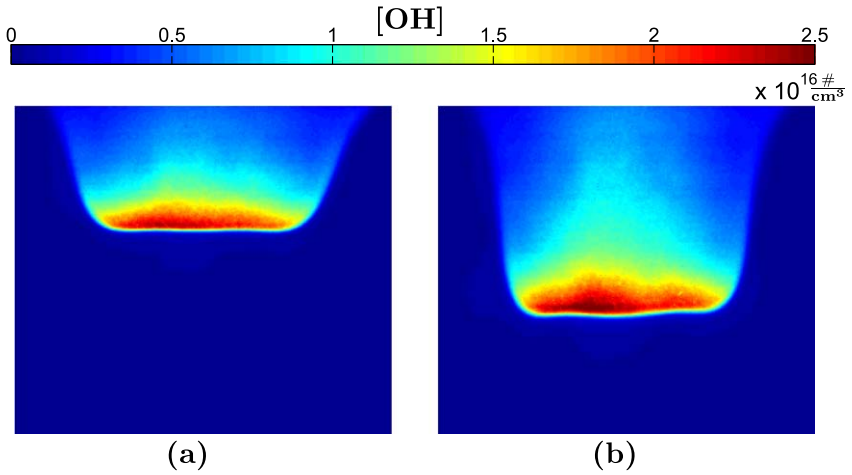

Fig. 7. Images of OH-number density in a ϕ = 0.76 CH_4/air flame without (a) and with (b) microwave enhancement.

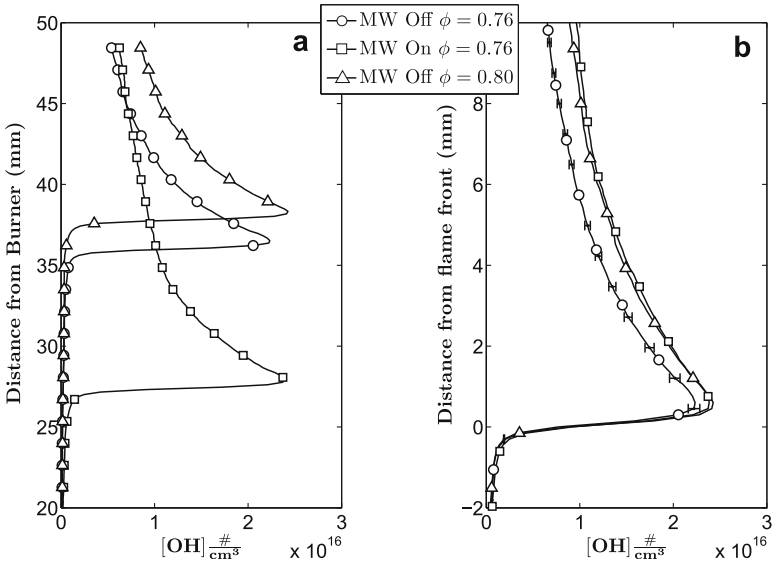

Fig. 8. OH-number density profiles showing the effect of microwave coupling on both peak OH concentration and the decay rate of OH towards equilibrium. (a) Absolute coordinate frame showing enhanced flame position. (b) Flame shifted coordinate system displaying non-enhanced flame (circles) with error bars, and the microwave enhanced OH profile (squares) matching to that of a flame that is less lean (triangles).

A typical result from the OH–PLIF experiments on the microwave enhanced flame system is shown in Fig. 8 for a $\phi = 0.76$, CH_4/air flame. For comparison, a measured profile for a non-microwave enhanced $\phi = 0.80$ flame is also shown. As can be seen in Fig. 8a, the OH profiles track not only the location of the flame front, but also the rate at which the OH radical decays from its superequilibrium peak. The sharp gradient in OH at the reaction zone can be used as a marker for flame location, and the shift of 8.6 mm in flame location with microwave coupling corresponds to the 14% flame speed enhancement and approximate 150 K increase in post-flame gas temperature reported in Figs. 4 and 6, respectively.

By aligning the flames in a flame centered coordinate system as in Fig. 8b, an increase in peak OH concentration of 6.5% can be observed. Along with this change in the superequilibrium peak of OH in the reaction zone, the OH profile of the microwave enhanced flame has a slower characteristic decay rate than what was seen without the microwave field. The rate of decay of OH-number density from the superequilibrium peak decreases with increasing equivalence ratio. With the application of microwave radiation to premixed CH_4/air flames, an enhancement of the OH decay rate from its peak value could be matched to those of a flame several hundredths of an equivalence ratio closer to the stoichiometric condition. For the case of a $\phi = 0.76$ flame presented in Fig. 8b, the concentration of OH along the axis of a microwave enhanced flame can be seen to align well with the experimental profile of a $\phi = 0.80$ flame. This increase in peak OH concentration and the matched alignment of the OH profile with stronger burning flames occurred for every equivalence ratio studied in the PLIF experimental set.

For the flames studied between equivalence ratios of 0.65 and 0.8, the increase in peak OH concentration is shown Fig. 9. The enhancement is well beyond the standard deviation of the measurements. The percentage increase in OH concentration is not as large as those enhancements measured in flame speed and temperature. The mechanism of this increase appears to have taken its effect through a modification of the superequilibrium of OH, which is typically characterized by two-body production rates being faster than the destructive three-body recombination in the region of peak heat release [28]. The further degree of superequilibrium measured in the microwave enhanced flame may be induced by subtle, but now relevant, charged species kinetics that will be investigated in future modeling efforts. Or more simply, the effect may be a result of the destructive three-body rates becoming even more deficient when number density decreases with the observed temperature increases in the microwave enhanced flame. The fact that this enhancement occurs in the narrow flame front region hints that the microwave interaction is imparting its effect through an interaction in the faster reacting portion of the flame to generate the measured increase in laminar flame speed.

4. Conclusions

A resonant microwave cavity was used to show that microwave fields have the ability to interact with combusting hydrocarbon systems to provide enhancement in laminar flame speed. Laser diagnostics were performed on a carefully designed microwave enhanced combustion testbed to yield datasets that document

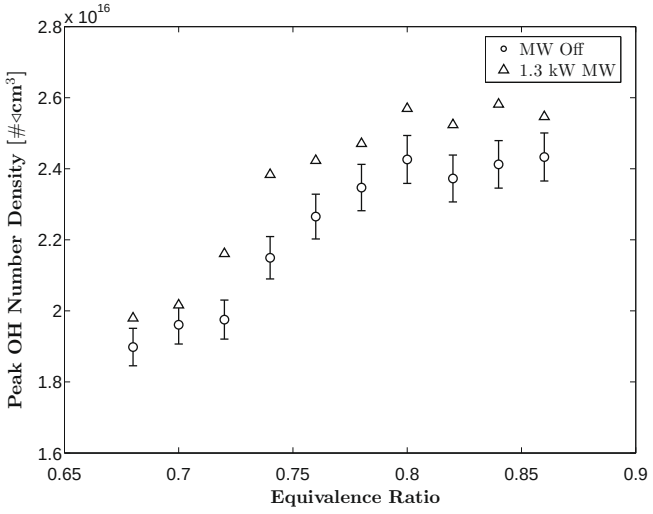

Fig. 9. Measured values of average peak OH concentration in CH_4/air flames with and without 1.3 kW microwave radiation enhancement vs. equivalence ratio.

the magnitude of the effect. From the experimental diagnostics presented in this article it is clear that the resonant microwave electric field is able to couple with the reacting flow of a premixed, CH_4/air flat, stagnation flame. The results from PIV demonstrate that the restabilization of the flame with the application of microwave radiation leads to an increase in its laminar flame speed of up to 20%. Temperature profiles measured by FRS reveal that thermal enhancements of 100–200 K occur and equilibrate just a few millimeters after the narrow the flame front. The FRS measurements also led to the conclusion that 20–40 W of microwave energy are absorbed into the enhanced flame from the 5 kV/cm electric field. Diagnostics with OH–PLIF show an increase in peak OH-number density and give reasonable credence to the hypothesis that the enhanced flame speed comes from a microwave interaction within the flame front.

Acknowledgments

Initial support for this research was provided by Research Science Instruments and the Air Force Office of Scientific Research (AFOSR) through an STTR under technical monitor, Dr. Julian Tishkoff. Emanuel Stockman thanks the Air Force Research Laboratory Summer Scholar Program and the Princeton Program in Plasma Sciences and Technology for graduate funding, as well as Dr. Philip Efthimion for his expertise and the lending of his microwave equipment. The PIV measurements were performed using laser and camera equipment loaned by Professor Yiguang Ju at Princeton University.

References

[1] H.C. Jaggers, A. von Engel, Combust. Flame 16 (1971) 275–285.
[2] R.J. Bowser, F.J. Weinberg, Combust. Flame 18 (2) (1972) 296–300.
[3] M.A.V. Ward, T.T. Wu, Combust. Flame 32 (1978) 57–71.
[4] C.S. MacLatchy, R.M. Clements, P.R. Smy, Combust. Flame 45 (1982) 161–169.
[5] E.G. Groff, M.K. Krage, Combust. Flame 56 (1984) 293–306.
[6] T. Pedersen, R.C. Brown, Combust. Flame 94 (1993) 433–448.
[7] D.L. Wisman, S.D. Marcum, B.N. Ganguly, Combust. Flame 151 (4) (2007) 639–648.
[8] H.F. Calcote, R.N. Pease, Ind. Eng. Chem. 43 (12) (1951) 2726–2731.
[9] R.G. Fowler, S.J.B. Corrigan, Phys. Fluids 9 (10) (1966) 1971.
[10] R.M. Clements, R.D. Smith, P.R. Smy, Combust. Flame 26 (1981) 77.
[11] S. Ogawa, Y. Sakai, K. Sato, S. Sega, Jpn. J. Appl. Phys. 1 (1) (1998) 179–185.
[12] A.Y. Starikovskii, Proc. Combust. Inst. 30 (2) (2005) 2405–2417.
[13] S.D. Marcum, B.N. Ganguly, Combust. Flame 143 (1-2) (2005) 27–36.
[14] Y. Ju, S.O. Macheret, M.N. Shneider, R.B. Miles, D.J. Sullivan, Numerical study of the effect of microwave discharge on the premixed methane–air flame, in: 40th AIAA/ASME/SAE/ASEE Joint Propulsion Conference and Exhibit, Fort Lauderdale, FL, 2004.
[15] S.H. Zaidi, E. Stockman, X. Qin, Z. Zhao, S. Macheret, Y. Ju, R.B. Miles, D.J. Sullivan, J.F. Kline, Measurements of hydrocarbon flame speed enhancement in high-Q microwave cavity, in: 44th AIAA Aerospace Sciences Meeting and Exhibit, Reno, Nevada, 2006, pp. 2006–1217.
[16] F.N. Egolfopoulos, H. Zhang, Z. Zhang, Combust. Flame 109 (1) (1997) 237–252.
[17] O.P. Gandhi, Microwave Engineering and Applications, Pergamon Press, New York, 1981.
[18] A. Ata, J.S. Cowart, A. Vranos, B.M. Cetegen, Combust. Sci. Technol. 177 (7) (2005) 1291–1304.
[19] Y. Dong, C.M. Vagelopoulos, G.R. Spedding, F.N. Egolfopoulos, Proc. Combust. Inst. 29 (2) (2002) 1419–1426.
[20] T. Hirasawa, C.J. Sung, A. Joshi, Z. Yang, H. Wang, C.K. Law, Proc. Combust. Inst. 29 (2) (2002) 1427–1434.
[21] M. Raffel, C.E. Willert, J. Kompenhans, Particle Image Velocimetry: A Practical Guide, Springer-Verlag, 1998.
[22] C.J. Sung, J.S. Kistler, M. Nishioka, C.K. Law, Combust. Flame 105 (1–2) (1996) 189–201.
[23] R.B. Miles, J.N. Forkey, W.R. Lempert, Filtered Rayleigh Scattering Measurements in Supersonic/Hypersonic Facilities, Nashville, TN, 1992.
[24] G.S. Elliott, N. Glumac, C.D. Carter, A.S. Nejad, Combust. Sci. Technol. 125 (1) (1997) 351–369.
[25] X. Pan, M.N. Shneider, R.B. Miles, Phys. Rev. A 69 (3) (2004) 33814.
[26] T. Ombrello, X. Qin, Y. Ju, A. Gutsol, A. Fridman, C. Carter, AIAA J. 44 (1) (2006) 142–150.
[27] Q.V. Nguyen, R.W. Dibble, C.D. Carter, G.J. Fiechtner, R.S. Barlow, Combust. Flame 105 (1996) 499–510.
[28] C.K. Law, C.J. Sung, G. Yu, R.L. Axelbaum, Combust. Flame 98 (1–2) (1994) 139–154.